Gene Expression Patterns and Tumor Uptake of ^{18}F-FDG, ^{18}F-FLT, and ^{18}F-FEC in PET/MRI of an Orthotopic Mouse Xenotransplantation Model of Pancreatic Cancer

Corinna von Forstner*[1], Jan-Hendrik Egberts*[2], Ole Ammerpohl[2], Dagmara Niedzielska[3], Ralph Buchert[3], Pal Mikecz[3], Udo Schumacher[4], Kersten Peldschus[5], Gerhard Adam[5], Christian Pilarsky[6], Robert Grutzmann[6], Holger Kalthoff[2], Eberhard Henze[1], and Winfried Brenner[3]

[1]Department of Nuclear Medicine, University Hospital of Schleswig-Holstein, Campus Kiel, Kiel, Germany; [2]Department of General Surgery and Thoracic Surgery, University Hospital of Schleswig-Holstein, Campus Kiel, Kiel, Germany; [3]Department of Nuclear Medicine, University Medical Center Hamburg-Eppendorf, Hamburg, Germany; [4]Department of Anatomy II Experimental Morphology, University Medical Center Hamburg-Eppendorf, Hamburg, Germany; [5]Department of Diagnostic and Interventional Radiology, University Medical Center Hamburg-Eppendorf, Hamburg, Germany; and [6]Department of Visceral, Thoracic, and Vascular Surgery, University Hospital Carl Gustav Carus, Technical University of Dresden, Dresden, Germany

Our aim was to use PET/MRI to evaluate and compare the uptake of ^{18}F-FDG, 3-deoxy-3-^{18}F-fluorothymidine (^{18}F-FLT), and ^{18}F-fluorethylcholine (^{18}F-FEC) in human pancreatic tumor cell lines after xenotransplantation into SCID mice and to correlate tumor uptake with gene expression of membrane transporters and rate-limiting enzymes for tracer uptake and tracer retention. **Methods:** Four weeks after orthotopic inoculation of human pancreatic carcinoma cells (PancTuI, Colo357, and BxPC3) into SCID mice, combined imaging was performed with a small-animal PET scanner and a 3-T MRI scanner using a dedicated mouse coil. Tumor-to-liver uptake ratios (TLRs) of the tracers were compared with gene expression profiles of the tumor cell lines and both normal pancreatic tissue and pancreatic tumor tissue based on gene microarray analysis and quantitative polymerase chain reaction. **Results:** ^{18}F-FLT showed the highest tumor uptake, with a mean TLR of 2.3, allowing correct visualization of all 12 pancreatic tumors. ^{18}F-FDG detected only 4 of 8 tumors and had low uptake in tumors, with a mean TLR of 1.1 in visible tumors. ^{18}F-FEC did not show any tumor uptake. Gene array analysis revealed that both hexokinase 1 as the rate-limiting enzyme for ^{18}F-FDG trapping and pancreas-specific glucose transporter 2 were significantly downregulated whereas thymidine kinase 1, responsible for ^{18}F-FLT trapping, was significantly upregulated in the tumor cell lines, compared with normal pancreatic duct cells and pancreatic tumor tissue. Relevant genes involved in the uptake of ^{18}F-FEC were predominantly unaffected or downregulated in the tumor cell lines. **Conclusion:** In comparison to ^{18}F-FDG and ^{18}F-FEC, ^{18}F-FLT was the PET tracer with the highest and most consistent uptake in various human pancreatic tumor cell lines in SCID mice. The imaging results could be explained by gene expression patterns of membrane transporters and enzymes for tracer uptake and retention as measured by gene array analysis and quantitative polymerase chain reaction in the respective cell lines. Thus, standard molecular techniques provided the basis to help explain model-specific tracer uptake patterns in xenotransplanted human tumor cell lines in mice as observed by PET.

Key Words: pancreatic carcinoma; ^{18}F-fluorodeoxyglucose; ^{18}F-fluorothymidine; ^{18}F-fluorethylcholine; MRI; PET; SCID mice; orthotopic xenotransplantation model; gene array

J Nucl Med 2008; 49:1362–1370
DOI: 10.2967/jnumed.107.050021

Pancreatic ductal adenocarcinoma (PDAC) is often detected at an advanced tumor stage, which, among other reasons, contributes to its dismal prognosis. The only curative option, radical surgical resection (Kausch-Whipple procedure) combined with lymphadenectomy, can raise the 5-y-survival rates to 20%–30% (*1,2*).

Suitable animal models that mimic the clinical situation as closely as possible are essential for developing and comparing new diagnostic and therapeutic strategies. Recently, we developed and described a clinically adapted orthotopic xenotransplantation model of pancreatic cancer that reflects the clinical situation in terms of local growth and metastasis (*3*). This model allows systematic preclinical in vivo testing of any new diagnostic and therapeutic option.

For both early staging and precise treatment monitoring, reliable diagnostic tools are mandatory. Abdominal or endoscopic ultrasonography with or without fine-needle aspiration,

Received Dec. 19, 2007; revision accepted Apr. 22, 2008.
For correspondence or reprints contact: Winfried Brenner, University Medical Center Hamburg-Eppendorf, Martinistrasse 52, 20246 Hamburg, Germany.
E-mail: winbren_2000@yahoo.com
*Contributed equally to this work.
COPYRIGHT © 2008 by the Society of Nuclear Medicine, Inc.

CT, MRI, and endoscopic retrograde cholangiopancreatography are the most frequently used diagnostic procedures for evaluation of patients in whom pancreatic cancer is clinically suspected (*4,5*). However, these methods have their limitations in distinguishing pancreatic cancer from chronic mass-forming pancreatitis and in differentiating viable tumor from posttherapeutic changes during follow-up (*5,6*).

PET with ^{18}F-FDG has been demonstrated to be useful in evaluating indeterminate pancreatic masses, staging pancreatic cancer, detecting metastatic disease, and differentiating viable tumor from posttherapeutic changes (*7–9*). However, although critical, the differentiation of pancreatic malignancy from focal pancreatitis, as well as tumor detection in cases of coexisting pancreatitis, is still a challenge by means of ^{18}F-FDG PET (*10*).

Shields et al. first reported the potential utility of 3-deoxy-3-^{18}F-fluorothymidine (^{18}F-FLT) for the noninvasive detection of cell proliferation using PET (*11*). ^{18}F-FLT is transported through the cell membrane and trapped inside the cell after phosphorylation by thymidine kinase 1 (TK1). Although ^{18}F-FLT is not incorporated into the DNA, it is still considered a surrogate marker of cellular proliferation because TK1 activity is closely regulated by the cell cycle (*12*). A close relationship between ^{18}F-FLT tumor retention and cell proliferation could be demonstrated, suggesting that ^{18}F-FLT is a promising marker for monitoring treatment response (*13,14*). In contrast to ^{18}F-FDG, ^{18}F-FLT is not taken up by inflammatory cells (*15*), potentially reducing the rate of false-positive findings both in pancreatitis and in inflammatory tissue after therapy.

Another PET tracer that recently came into the focus of tumor imaging is ^{18}F-fluorethylcholine (^{18}F-FEC). PET with choline was first introduced for the evaluation of brain tumors (*16*) and more recently was examined for imaging prostate cancer and esophageal carcinoma (*17,18*). Choline is incorporated into cells through phosphoryl choline synthesis and subsequent integration into membrane phospholipids (*19*). Increased choline uptake therefore is expected in proliferating tumor cells. Thus, ^{18}F-FEC is also considered a kind of proliferation marker, although uptake mechanisms and biochemical features are completely different from those of ^{18}F-FLT.

The aim of our animal study was twofold: first, to use PET/MRI to evaluate and compare the uptake of ^{18}F-FDG, ^{18}F-FLT, and ^{18}F-FEC in human pancreatic tumor cell lines after orthotopic xenotransplantation into SCID mice, and second, to use gene array analysis and quantitative polymerase chain reaction (qPCR) to correlate tumor uptake with gene expression of membrane transporters and rate-limiting enzymes for tracer uptake and tracer retention. Based on these data, we wanted to learn more about the molecular basis for tracer uptake in our pancreatic tumor mouse model with respect to model-inherent conditions as a basis for future studies on new treatment approaches.

MATERIALS AND METHODS

Preparation of Radiopharmaceuticals

^{18}F-FDG was synthesized in a commercial synthesis module (Nuclear Interface) using a modification of the technique described by Hamacher et al. (*20*).

^{18}F-FLT was synthesized using 3-*N*-Boc-5′-*O*-dimethoxytrityl-3′-*O*-nosyl-thymidine (ABX; Advanced Biochemical Compounds) as a precursor for use in a synthesis module developed in-house. The precursor reacted with the ^{18}F fluoride ions in the presence of Kryptofix 2.2.2 (Merck) phase transfer catalyst in acetonitrile at 130°C. After subsequent hydrolysis with 1 M hydrochloric acid, ^{18}F-FLT was purified on a semipreparative Nucleodur Pyramid C18 high-performance liquid chromatography column (Macherey-Nagel). The column was eluted with a mobile phase of 7.5% ethanol in 0.015 M phosphate buffer (pH 5.5). The final product had a specific activity of 2–5 GBq/μmol, with a radiochemical purity of more than 99%.

^{18}F-FEC was synthesized by a 2-step 1-pot method similar to that of Hara et al. (*21*). First, the dried ^{18}F fluoride ions reacted with 1,2 bis(tosyloxy)ethane (Fluorochem Ltd.) in the presence of Kryptofix 2.2.2 phase transfer catalyst in acetonitrile at 80°C. After the reaction was completed, the acetonitrile was evaporated at 60°C with helium flow, yielding 2-^{18}F-fluoroethyl tosylate. Subsequently, 0.5 mL of di-methyl-aminoethanol was added. The second reaction took place at 100°C, resulting in ^{18}F-FEC. The unreacted precursor was evaporated at 130°C. The dried residue was dissolved in 2 mL of water and passed through a cation exchange cartridge (Sep-Pak Accell Plus CM; Waters Corp.). The cartridge was washed with 10 mL of ethanol and 10 mL of water subsequently, and ^{18}F-FEC was eluted with 5 mL of saline solution from the cartridge. After sterile filtration, the ready-to-use product had a radiochemical purity of more than 99%.

Laboratory Animals

Four-week-old female SCID beige mice weighing 14–19 g were obtained from Harlan-Winkelmann. The mice were allowed to become acclimatized for 10 d and were housed in a sterile environment in which bedding, food, and water had been autoclaved (Scantainer). Animal experiments and animal care were in accordance with the guidelines of institutional committees and approved by local ethics and radiation safety authorities.

Tumor Cell Preparation and Orthotopic Xenotransplantation

Three different human ductal pancreatic adenocarcinoma cell lines (BxPc3, Colo357, and PancTuI) were investigated. These cells were different in their origin (BxPc3 and PancTuI were generated from a primary tumor, Colo357 from lymph node metastasis), their primary histologic grade (BxPc3, G2; Colo357, G1–G2; and PancTuI, G2–G3), and genetic aberrations as published elsewhere (*22*). The cells were routinely cultured in RPMI-1640 medium, supplemented with 10% fetal calf serum (PAN-Systems) and 2 mM glutamine (Life Technologies). The cells were maintained at 37°C in a humid atmosphere with 5% CO_2. For orthotopic transplantation, the cells were trypsinized and suspended in Matrigel (BD Bioscience) at a concentration of 10^6 cells/mL and stored on ice. The viability of the cells was confirmed by trypan blue dye exclusion testing. After median laparotomy, 30 μL of tumor cell suspension were injected into the pancreatic body to the left of the organ midline.

PET and MRI

Imaging was performed 4 wk after orthotopic inoculation of the tumor cells. Two subsets of mice had been kept fasting overnight before imaging with ^{18}F-FDG, and all the other animal subsets were fed ad libitum. Several mice were imaged with 2 or all 3 tracers within 1 wk for direct comparison of tracer uptake. All tracers were injected via the tail vein, with the total injected volume being no more than 0.2 mL. To stimulate voiding of the bladder, 1 mg of furosemide was injected intraperitoneally. Twenty-five minutes after tracer injection, the animals were anesthetized by intraperitoneal injection of a combination of fentanyl, midazolam, and medetomidine, with dosages of 0.05, 5, and 0.5 mg/kg, respectively. Each mouse was separately positioned on a special mouse bed composed of polyvinyl chloride and suitable for consecutive MRI and PET without repositioning of the animal.

MRI was performed on a clinical 3.0-T whole-body MRI scanner (Intera; Philips) equipped with a standard gradient system (gradient strength, 40 mT/m). For signal exploitation, a dedicated small-animal solenoid coil (Philips Research) with an inner diameter of 40 mm and an integrated heating system to regulate the body temperature of the mice during MRI scans was used. The MRI protocol consisted of a T1-weighted survey scan and a T2-weighted 2-dimensional turbo spin-echo sequence in the coronal orientation. The scan parameters were as follows: repetition time, 6,551 ms; echo time, 90 ms; echo train length, 10; field of view, 90 × 45 mm; matrix, 384 × 192 pixels; number of slices, 36; number of acquisitions, 3. The effective in-plane resolution was 230 × 230 μm, with a slice thickness of 700 μm. The total scanning time was 12 min and 39 s.

After the MRI scan, the mouse bed with the anesthetized animal was transferred to the PET unit and positioned on the bed of a Mosaic small-animal PET system (Philips). The scanner operates exclusively in 3-dimensional mode with a sensitivity of 0.65% and a spatial resolution of approximately 3 mm in full width at half maximum at the center of the system (*23*). The coincidence timing window was 12 ns, and a standard energy window of 410–665 keV was used. PET imaging started at 60 min after tracer injection, independent of the tracer. Data were acquired for 10 min, resulting in a sinogram containing the detected coincidences, corrected for randoms. Sinograms were reconstructed into a 128 × 128 matrix (1 × 1 × 1 mm voxel size) of transaxial images using the 3-dimensional row-action maximum-likelihood algorithm. Data corrections included normalization, and correction for dead-time and decay. No corrections were made for attenuation or scatter.

The MRI and PET scans were coregistered and fused by rigid-body transformations using PMOD software (version 2.8; PMOD Technologies). The perpendicular long- and short-axis diameters of the tumors were measured on MR images, and tumor volume was calculated on the basis of an ellipsoid model by PMOD software. Only the solid parts of the tumors were used for diameter measurements; cystic portions of the tumors were excluded.

In visible tumors, tracer uptake was expressed as tumor-to-liver uptake ratio (TLR). Because of the limited resolution of the PET system, we had to choose a reference region with diameters of at least 6 mm to avoid substantial partial-volume effects. Therefore, the liver was chosen as the only possible single organ or tissue large enough, although we know that tracer uptake in the liver depends on various factors including time after injection, which was kept constant in all cases. For calculating the TLR, a region of interest was placed in the tumor plane with the highest tumor uptake, and the maximum activity within this region of interest was used for calculation. For the liver, a circular region of interest was placed in the center plane, and the mean activity of this region of interest was used as the reference.

qPCR Analysis

RNA from all 3 pancreatic carcinoma cell lines and peripheral blood lymphocytes from 3 healthy human donors were isolated using the Microto-Mini Total RNA Purification Kit (Invitrogen). Reverse transcription was performed using Superscript II reverse transcriptase (Invitrogen) and random hexamers (Roche). Relative messenger RNA levels were determined by qPCR performed with IQ SYBR Green Supermix (Bio-Rad) and analyzed by the Opticon real-time PCR system using MJ Opticon Monitor Analysis Software (Bio-Rad). The following primers were used (5′-3′): human TK1 sense, GCTTCCAGATTGCTCAGTAC; TK1 antisense, GGCACCAGGTTCAGGATG; glucose-6-phosphate dehydrogenase sense, ACGTGATGCAGAACCACCTACTG; and glucose-6-phosphate dehydrogenase antisense, ACGACGGCTGCAAAAGTGGCG.

Gene Array Analysis

To determine the impact of aberrant gene expression in pancreatic cancer cell lines on the uptake of the different tracers in our animal model, we investigated the expression profile of genes known to be involved in membrane transport and metabolism of the tracers.

^{18}F-FDG. SLC2A1 (solute carrier family 2 [facilitated glucose transporter] member 1) (GLUT1), SLC2A10 (GLUT10), SLC2A11 (GLUT11), SLC2A12 (GLUT12), SLC2A13 (HMIT), SLC2A2 (GLUT2), SLC2A3 (GLUT3), SLC2A4 (GLUT4), SLC2A5 (GLUT5), SLC2A6 (GLUT6), SLC2A8 (GLUT8), SLC2A9 (GLUT9), SLC5A10 (SGLT5), SLC5A11 (SGLT6), SLC5A4 (SGLT3), SLC5A9 (SGLT4), and HK1 (hexokinase 1).

^{18}F-FLT. SLC28A1 (CNT1), SLC28A2 (CNT2), SLC28A3 (CNT3), SLC29A1 (ENT1), SLC29A2 (ENT2), SLC29A3 (ENT3), SLC29A4 (ENT4), DTYMK (deoxythymidylate kinase), and TK1.

^{18}F-FEC. CHKA (choline kinase α), CHKB (choline kinase β), PCYT1A (phosphate cytidylyltransferase 1, choline, α), PCYT1B (phosphate cytidylyltransferase 1, choline, β), PLCB1 (phospholipase C, β-1), PLCB4 (phospholipase C, β-4), PLCD3 (phospholipase C, δ-3), PLCD4 (phospholipase C, δ-4), PLCG1 (phospholipase C, γ-1), PLD1 (phospholipase D1), SLC18A3 (VACHT), SLC44A1 (CTL1), and SLC5A7 (CHT).

We analyzed and compared the expression data obtained from a previously published study based on Affymetrix microarray analysis (*24*) specifying the gene expression profiles from 19 microdissected PDAC directly obtained from patients, 13 microdissected normal pancreatic ducts, and numerous pancreatic carcinoma cell lines including Colo357, PancTuI, and BxPc3.

Statistical Analysis

Intersubject effects of tumor entity (Colo357, PancTuI, and BxPc3) and tracer (^{18}F-FDG and ^{18}F-FLT) on TLR were tested by univariate ANOVA using SPSS (version 14.0 for Windows [Microsoft]; SPSS Inc.). To assess the potential impact of variable partial-volume effects caused by differences in tumor volume, we repeated ANOVA with tumor volume as covariate. An effect was considered statistically significant if it reached the 2-sided 0.05 level. The Student *t* test was performed for statistical evaluation of gene array analysis using GraphPad Prism 4.02 (GraphPad Software).

RESULTS

Tumor Tracer Uptake of ^{18}F-FDG, ^{18}F-FLT, and ^{18}F-FEC

^{18}F-FDG allowed visualization of 4 of 8 pancreatic tumors (50%), and tumor uptake was low, with a mean TLR of 1.1 in visible tumors (Table 1). ^{18}F-FDG showed uptake in 3 of 4 PancTuI tumors and in 1 of 2 BxPc3 tumors. There was no ^{18}F-FDG uptake in Colo357 tumors. No significant differences in TLRs were found between fasting and nonfasting animals ($P = 0.183$).

^{18}F-FLT allowed correct visualization of all 12 pancreatic tumors (100%), with a significantly higher mean TLR of 2.3 (Table 2) than was obtained with ^{18}F-FDG or ^{18}F-FEC. In particular, ^{18}F-FLT showed a higher TLR than did ^{18}F-FDG in all tumors but 1 Colo357 tumor, with the differences increasing from PancTuI (12%) to Colo357 (93%) to BxPc3 (376%). All effects were highly statistically significant according to ANOVA (tumor, $P = 0.001$; tracer, $P < 0.0001$; tumor–tracer interaction, $P < 0.0001$). These results were confirmed by the repeated ANOVA with tumor volume as covariate (tumor, $P = 0.004$; tracer, $P = 0.001$; tumor–tracer interaction, $P = 0.004$). Tumor volume had no effect ($P = 0.484$) on tracer uptake. Figure 1 demonstrated high ^{18}F-FLT uptake in a BxPc3 tumor, whereas in the same tumor, relevant uptake of neither ^{18}F-FDG nor ^{18}F-FEC could be observed.

^{18}F-FEC showed no tumor uptake in any of the 10 pancreatic tumors investigated (Table 3).

Biodistribution of ^{18}F-FDG, ^{18}F-FLT, and ^{18}F-FEC

^{18}F-FDG revealed physiologic tracer uptake in the heart, brain, brown fat of the shoulder girdle area, liver, and urinary system (with bladder), as well as limited uptake in half the tumors (Fig. 1A). ^{18}F-FLT accumulated in the gallbladder, kidneys, and bladder, with relatively high physiologic uptake in the liver and high uptake in all pancreatic tumors (Fig. 1B). Physiologic uptake of ^{18}F-FEC was found in the liver, cortex of the kidneys, and duodenum, whereas no tumor uptake could be detected as confirmed by coregistered PET/MRI (Fig. 1C).

TABLE 1
Tumor Uptake of ^{18}F-FDG in the Different Pancreatic Tumors

Tumor	Activity (MBq)	Body weight (g)	Volume (mL)	TLR
PancTul 1	13.2	21.4	0.53	0
PancTul 2	15.4	16.7	1.49	1.2
PancTul 3	11.0	18.6	1.89	1.1
PancTul 4	13.6	17.2	1.24	1.3
Colo357 1*	20.2	18.5	0.24	0
Colo357 2*	15.6	19.2	0.08	0
BxPc3 1*	20.3	17.6	0.48	0
BxPc3 2*	21.3	18.3	0.35	0.9
Mean	16.3	18.4	0.79	0.6
SD	3.8	1.4	0.66	0.6

*Fasting animals.

TABLE 2
Tumor Uptake of ^{18}F-FLT in the Different Pancreatic Tumors

Tumor	Activity (MBq)	Body weight (g)	Volume (mL)	TLR
PancTul 5	10	15.2	0.82	1.3
PancTul 6	11	17.4	0.71	1.6
PancTul 7	11	19.0	1.33	1.6
PancTul 8	11	17.1	1.48	1.7
Colo357 3	25	18.4	0.06	1.5
Colo357 4	24	17.8	0.07	2.0
Colo357 5	23	17.9	0.04	1.6
Colo357 6	24	16.5	0.12	1.2
Colo357 1	24	16.8	0.24	2.4
BxPc3 3	25	18.6	0.36	3.4
BxPc3 1	21	18.9	0.48	5.4
BxPc3 2	22	17.4	0.35	4.0
Mean	19	17.6	0.51	2.3
SD	6.4	1.1	0.49	1.3

MRI and Image Fusion

MRI and image fusion were mandatory for exact tumor delineation and, thus, for PET image interpretation in mice with no clear tracer uptake in tumors. Fused images were also helpful in cases of tumor uptake near organs with pronounced physiologic tracer uptake, such as ^{18}F-FDG within the kidneys or ^{18}F-FLT in the gallbladder. For example, in Figure 1 it is hard to define the exact extension of tumor uptake on the PET images, even with the help of MRI. Fused images, however, easily allow the delineation of tumor uptake and its differentiation from surrounding tissue.

Measurements of tumor diameters on MR images revealed perpendicular long- and short-axis diameters ranging from 0.58 to 1.75 cm (mean, 1.20 cm) and 0.23 to 1.23 cm (mean, 0.66 cm), respectively. Tumor volumes are given in Tables 1–3.

Expression of Genes Involved in Uptake of ^{18}F-FDG, ^{18}F-FLT, and ^{18}F-FEC

The expression profile of the selected genes in the tumor cell lines was compared with the mean expression in 13 microdissected normal pancreatic ducts and 19 microdissected PDAC as shown in Figures 2–4.

Although the glucose transporter SLC2A1 (GLUT1) was upregulated in the tumor cell lines, compared with normal pancreatic tissue ($P = 0.0002$), SLC2A2 (GLUT2) and SLC2A10 (GLUT10) were significantly downregulated ($P = 0.0058$ and 0.0067, respectively). The latter one is in contrast to expression in PDAC samples, where no downregulation was found ($P = 0.1381$). SLC2A13 was expressed at a low level comparable to the expression level found in PDAC but with a lower mean value than observed in normal pancreatic tissue. Although HK1 was upregulated in PDAC, compared with normal pancreatic tissue ($P = 0.0113$), HK1 showed no aberrant expression patterns in the tumor cell lines. Other genes involved in the ^{18}F-FDG pathway were mainly downregulated or unaffected in the cell lines investigated.

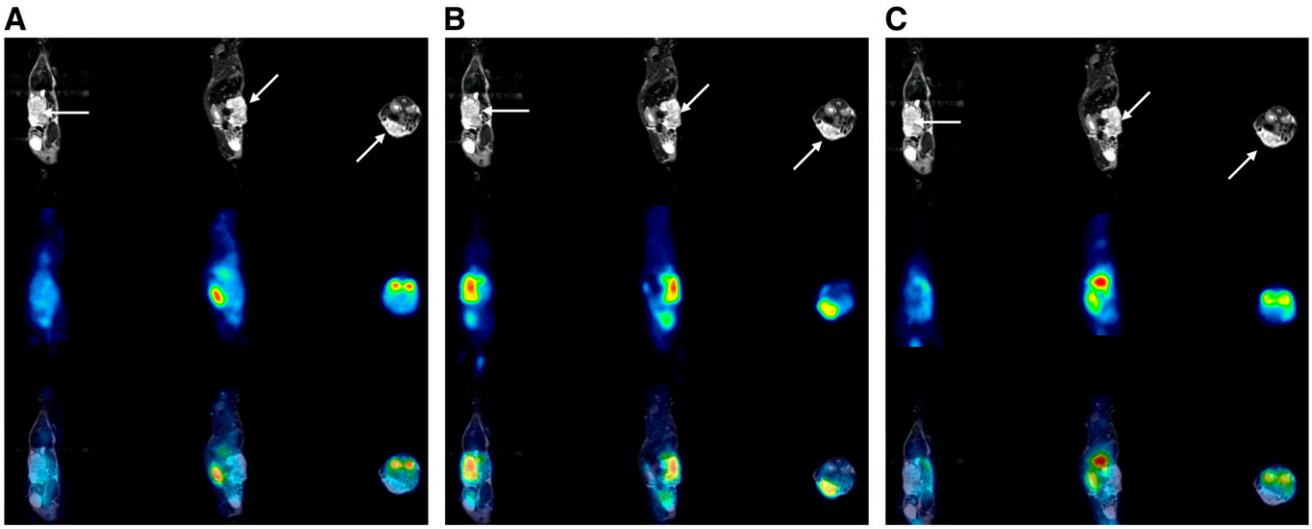

FIGURE 1. Tumor uptake of ^{18}F-FDG (A), ^{18}F-FLT (B), and ^{18}F-FEC (C) in mouse 1 with a BxPc3 tumor (row 1: MRI; row 2: PET; row 3: PET/MRI). Tumor is readily visible in abdomen on MR images (arrows). (A) There is no increased ^{18}F-FDG uptake within tumor; hot spots are ^{18}F-FDG activity within kidneys. (B) Tumor is readily visible, showing intense ^{18}F-FLT uptake that is higher than in any other organ. (C) There is no ^{18}F-FEC uptake within tumor; liver and kidneys show pronounced tracer uptake.

Thus, besides SLC2A1, no other gene of the ^{18}F-FDG pathway was upregulated in tumor cell lines (Fig. 2).

In line with the results obtained from PDAC, we found the sodium-coupled nucleoside transporter SLC28A1 and the nucleoside transporter SLC29A3 downregulated ($P = 0.0104$ and $P = 0.0170$, respectively) in all 3 tumor cell lines. In contrast, 2 kinases involved in the ^{18}F-FLT pathway, DTYMK ($P < 0.0001$) and TK1 ($P < 0.0001$), were upregulated in a highly significant way in the tumor cell lines but far less in the PDAC samples (not statistically significant; Fig. 3). By comparing the relative TK1 expression in the cell lines with the expression pattern obtained from peripheral blood lymphocytes from 3 healthy donors by qPCR, we found TK1 overexpressed in all tumor cell lines. Mean relative TK1 expression was 128 in PancTuI, 11 in Colo357, and 6 in BxPc3, compared with the mean expression in blood lymphocytes, which was set as 1.

Besides PLCD3, which was upregulated in the pancreatic tumor cell lines ($P < 0.0001$), other genes involved in the uptake of ^{18}F-FEC were predominantly unaffected or downregulated in the tumor cell lines, compared with their expression in normal duct cells or PDAC (Fig. 4). Although CHKA showed no aberrant expression patterns, CHKB was significantly ($P = 0.0182$) downregulated. PCYT1B, PLCB1, and PLD1 showed in all cell lines low expression levels comparable to PDAC (Fig. 4).

The expression patterns obtained from the pancreatic tumor cell lines used in our study were similar to those from PDAC samples obtained from patients for most of the genes investigated. Of special interest, however, is the finding that both HK1 as the rate-limiting enzyme for ^{18}F-FDG trapping and SLC2A10 (GLUT10) were significantly downregulated in the tumor cell lines, compared with PDAC samples (Fig. 2), whereas for ^{18}F-FLT, TK1, and DTYMK were significantly upregulated in the tumor cell lines, compared with PDAC samples (Fig. 3).

DISCUSSION

In this study on tumor uptake of various PET tracers in 3 different human pancreatic tumor cell lines orthotopically transplanted into the pancreas of SCID mice, we were able to detect all pancreatic tumors irrespective of the tumor type with ^{18}F-FLT, whereas with ^{18}F-FDG we could detect only half the tumors, and ^{18}F-FEC failed to detect any tumor.

^{18}F-FDG, an analog of glucose, is taken up by glucose transporters into cells and subsequently undergoes phosphorylation by the rate-limiting key enzyme HK1 into ^{18}F-FDG-monophosphate. Because tumors usually show increased glucose metabolism, ^{18}F-FDG became the tracer most widely used for PET in both oncology in general and in pancreatic cancer (*10*).

The rationale of using ^{18}F-FLT for visualization and quantification of cell proliferation is based on its substrate specificity for the cell cycle–regulated key protein, TK1, for which activity is stimulated at the G_1–S border (*25,26*). However, numerous factors are potentially related to an imperfect correlation between ^{18}F-FLT uptake and tumor cell proliferation. Loss of cell cycle–specific regulation of TK1 may result in ^{18}F-FLT uptake during the G_1 and G_2 phases (*27*), and tumor perfusion, vascular permeability, and nucleoside transporter activity may change ^{18}F-FLT uptake independently of cellular proliferation.

Based on the fact that most cancer cells are metabolically active but considerably fewer cells are proliferating at any given time, a higher net tumor uptake of ^{18}F-FDG than of ^{18}F-FLT can be expected. Besides tumor cells, many inflammatory cells are usually present in malignant lesions, further contributing to ^{18}F-FDG uptake in tumors (*28*). Thus, in

TABLE 3
Tumor Uptake of ^{18}F-FEC in the Different Pancreatic Tumors

Tumor	Activity (MBq)	Body weight (g)	Volume (mL)	TLR
Colo357 1	22	18.4	0.24	0
Colo357 2	22	17.8	0.08	0
Colo357 7	25	17.9	0.12	0
Colo357 5	22	16.5	0.04	0
Colo357 4	25	16.8	0.07	0
BxPc3 3	28	18.6	0.36	0
BxPc3 1	22	18.9	0.48	0
BxPc3 4	24	17.4	0.25	0
BxPc3 5	23	19.6	0.27	0
BxPc3 6	21	18.5	0.65	0
Mean	23	18.0	0.26	0
SD	2	0.9	0.20	0

studies comparing the uptake of ^{18}F-FDG and ^{18}F-FLT in patients with tumors, tumor uptake is regularly higher for ^{18}F-FDG than for ^{18}F-FLT (*29,30*). These observations have been confirmed in many different tumor entities and in pancreatic cancer (*31*).

In our mouse model, uptake of ^{18}F-FLT in pancreatic cancer was significantly higher than that of ^{18}F-FDG and ^{18}F-FEC. Reviewing the literature on PET in mice, we found that several studies reported a lower tumor uptake of ^{18}F-FLT and a significantly higher uptake of ^{18}F-FDG, as is the case in patient studies. However, there are studies presenting contrary findings in mouse models, with significantly higher ^{18}F-FLT uptake than ^{18}F-FDG uptake in malignant human tumors such as neuroblastoma or squamous cell carcinoma (*32,33*).

Except for an upregulation of SLC2A1 (GLUT1), which is typically upregulated in most human cancers, both expression of other glucose transporters and expression of the rate-limiting enzyme HK1 were reduced or unchanged, compared with normal pancreatic cells. HK1 expression was similar to that of control cells but was decreased in comparison to that of PDAC samples. Surprisingly, we found a pronounced downregulation of pancreas-specific SLC2A2 (GLUT2) in all 3 cell lines. These expression patterns may explain the observation that ^{18}F-FDG was of only limited value for tumor detection in our animal model, depicting only 4 of 8 tumors (Table 1). These patterns might also explain why we did not observe a significant difference in ^{18}F-FDG tumor uptake between animals fed ad libitum and fasting animals, a finding that contradicts the findings published by Fueger et al. for imaging xenotransplanted tumors in mice by small-animal PET (*34*). In addition, inflammatory reactions within or around tumor tissue are reduced or absent in SCID mice because of their genetically restricted immunogenic capacity, which further contributes to a relatively lower ^{18}F-FDG tumor uptake than in patients.

Although several members of relevant transporter protein families for ^{18}F-FLT were downregulated to some extent, other nucleoside transporters were unchanged, suggesting that the ^{18}F-FLT influx is not restricted substantially. Moreover,

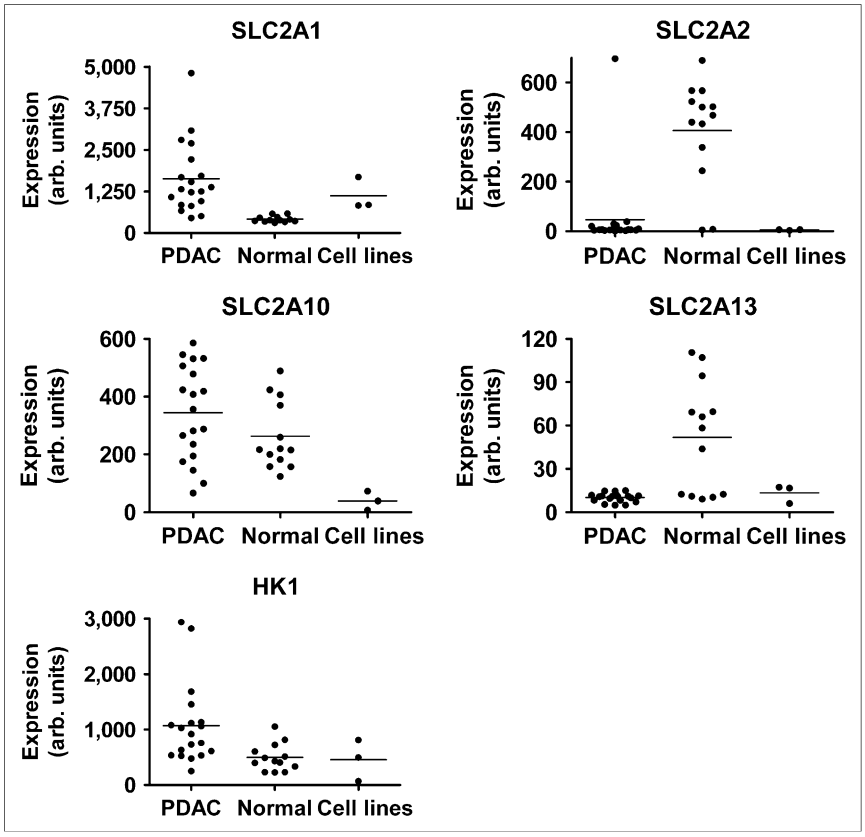

FIGURE 2. Expression of genes involved in membrane transport or metabolism of ^{18}F-FDG in pancreatic cancer cell lines PancTul, Colo357, and BxPc3, compared with expression in normal pancreatic duct cells (n = 13) and PDAC cells (n = 19) as determined by microarray analysis. Mean expression level is marked by a line.

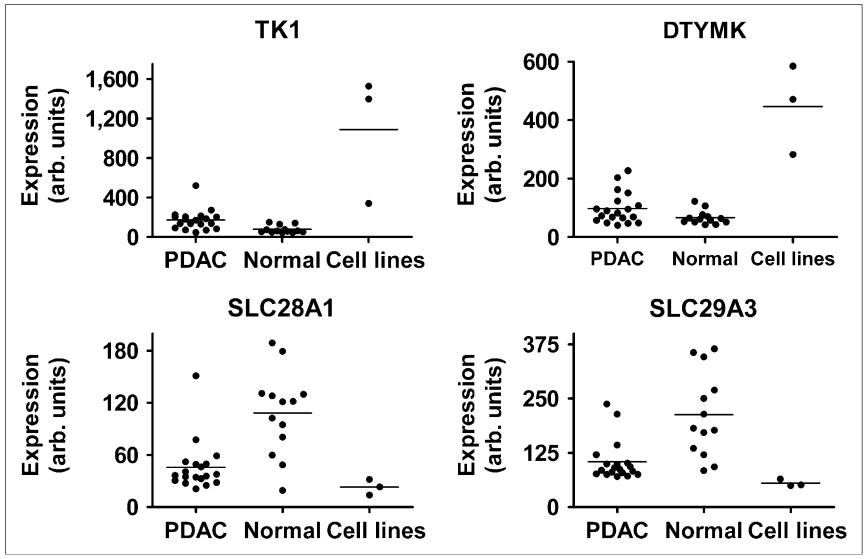

FIGURE 3. Expression of genes involved in membrane transport or metabolism of ^{18}F-FLT in pancreatic cancer cell lines PancTuI, Colo357, and BxPc3, compared with expression in normal pancreatic duct cells (n = 13) and PDAC cells (n = 19) as determined by microarray analysis. Mean expression level is marked by a line.

in all 3 pancreatic tumor cell lines we found highly increased levels of TK1 expression, compared with both normal pancreatic tissue and PDAC. These data indicate retention of a high percentage of ^{18}F-FLT due to increased phosphorylation by TK1 despite a putatively reduced initial ^{18}F-FLT uptake. Most human xenotransplanted tumor cells grow to more than 1 cm in diameter within 3–4 wk, and these tumors are characterized by high mitotic rates of up to 30%–70% (Winfried Brenner, unpublished data, 1989). Given a highly increased TK1 activity in a high percentage of proliferating tumor cells in SCID mice, high ^{18}F-FLT uptake can be expected as demonstrated by PET (Table 2; Fig. 1B).

Comparing the gene expression patterns between the tumor cell lines used in our model and PDAC samples directly obtained from patients, we found that HK1, as the rate-limiting enzyme for ^{18}F-FDG trapping, was significantly downregulated in the tumor cell lines, compared with PDAC (Fig. 2), whereas for ^{18}F-FLT TK1 and the kinase DTYMK

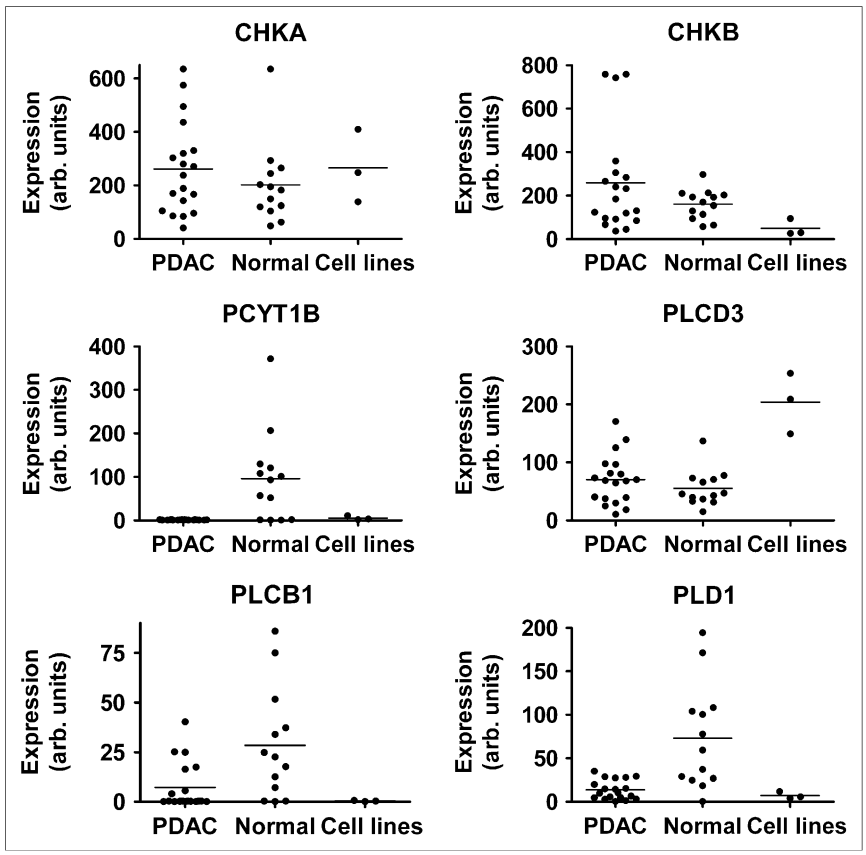

FIGURE 4. Expression of genes involved in membrane transport or metabolism of ^{18}F-FEC in pancreatic cancer cell lines PancTuI, Colo357, and BxPc3, compared with expression in normal pancreatic duct cells (n = 13) and PDAC cells (n = 19) as determined by microarray analysis. Mean expression level is marked by a line.

were significantly upregulated in the tumor cell lines, compared with PDAC tumor samples (Fig. 3). These differences in gene expression clearly explain the reverse uptake pattern of a significantly higher uptake of ^{18}F-FLT than of ^{18}F-FDG in our xenotransplanted human pancreatic tumor cells, in comparison to patient studies, which have usually reported a higher ^{18}F-FDG uptake than ^{18}F-FLT uptake.

In contrast to ^{18}F-FDG and ^{18}F-FLT, we did not find any significant tumor uptake of ^{18}F-FEC. High physiologic uptake is usually observed in the liver and the cortex of the kidneys and is furthermore observed in the duodenum and the pancreas because of secretion of phospholipid-rich pancreatic juice (*19,21*). High tumor uptake of ^{11}C-choline or ^{18}F-FEC has been reported for esophageal carcinoma (*18*), brain tumors (*16,35*), hepatocellular carcinoma (*36*), prostate cancer (*17,37*), and gynecologic malignancies (*38*). However, so far there have been no studies of ^{18}F-FEC PET in pancreatic cancer.

The mechanisms for cellular uptake of choline have not been completely clarified yet. Choline is transported into cells and acts as a precursor for the biosynthesis of phospholipids, which are constitutive elements of the lipid bilayer of cell membranes (*39*). Hara et al. reported in 2002 that ^{18}F-FEC is incorporated into tumor cells by active transport against a concentration gradient and is then phosphorylated inside the cells by choline kinase and subsequently by phosphocytidylyltransferase, yielding phosphoryl-^{18}F-FEC, and is finally integrated into phospholipids, probably primarily into phosphatidyl-^{18}F-FEC (*21*). These mechanisms constitute a kind of chemical trap. However, phospholipase activity can hydrolyze phospholipids such as phosphatidyl-^{18}F-FEC, resulting in a loss of membrane-bound ^{18}F-FEC.

In our study, we did not observe any tumor uptake of ^{18}F-FEC, not even in tumors with high ^{18}F-FLT uptake suggesting a high proliferative activity (Fig. 1). The expression patterns of ^{18}F-FEC–relevant transporters and enzymes, however, were not as clear as the results for ^{18}F-FLT and ^{18}F-FDG. Ubiquitous organic cationic transporters with low affinity for ^{18}F-FEC were only weakly expressed or were not aberrantly expressed at all in the 3 tumor cell lines. Various cholinelike transporters also did not show significant changes, compared with control pancreatic cells (data not shown). Expression of choline kinase A in BxPC3 and Colo357 tumors was either similar to that in normal pancreatic cells or slightly upregulated in PancTuI, whereas choline kinase B was rather downregulated. The other rate-limiting enzymes for phosphorylation of ^{18}F-FEC, the phosphocytidylyltransferases, were also downregulated or unchanged in all 3 tumor cell lines. Hydrolysis of ^{18}F-FEC from membrane phospholipids could at least in part explain the lack of ^{18}F-FEC retention in tumor cells (*40*). However, a better understanding of ^{18}F-FEC metabolism in general will be necessary to check for expression patterns of relevant transporters and enzymes in future studies. Another important factor still to clarify is the question of whether ^{18}F-FEC, an ethylated choline, is a substrate for the very same choline transporters and metabolic pathways as choline itself or whether ^{18}F-FEC shows differences in membrane transport and metabolism.

In our study, we combined PET and MRI by using a rigid-body transformation for image coregistration and fusion. This combination allows visualization of both whole-body anatomic and functional information within 1 set of 3-dimensional images without applying any further radiation to the animals, as is significantly the case for high-resolution micro-CT. In contrast to liver and bowel, tumors appear hyperintense on T2-weighted MR images because of the edematous tumor tissue. These images allowed a clear delineation of the tumor extension within the abdominal cavity, and the overlay of the MRI datasets facilitated the delineation of tumor uptake on PET images. This delineation was helpful—if not mandatory—for evaluating tumors near organs with physiologic tracer uptake, because on PET images alone the assessment of tumor uptake was hampered by intense organ uptake of the respective tracer as shown in Figure 1. Thus, combined PET/MRI with image fusion proved feasible and helpful for correct PET image interpretation in our mouse model with orthotopically xenotransplanted pancreatic tumors and seems to be a promising tool for further studies on monitoring therapy by measuring response in terms of changes in tumor tracer uptake and tumor volume.

CONCLUSION

In our xenotransplantation SCID mouse model, we found that ^{18}F-FLT was the PET tracer with the highest and most consistent tumor uptake in various orthotopically transplanted human pancreatic tumor cell lines, in comparison to ^{18}F-FDG and ^{18}F-FEC. The imaging results could be explained by gene expression patterns of membrane transporters and rate-limiting enzymes for tracer uptake and tracer retention as measured by gene array analysis and qPCR in the respective cell lines. Thus, standard molecular research tools provided the basis to explain and help us understand model-specific tumor uptake patterns as observed by PET. However, not only the combination of molecular analysis of tumor cells and PET but also the use of combined functional small-animal PET and morphologic high-resolution MRI helped to improve image interpretation in our mouse model of pancreatic cancer.

ACKNOWLEDGMENTS

We thank Cornelia Burger, Thomas Dreilich, and Florian Wilke for excellent technical assistance. This work was supported by the Deutsche Forschungsgemeinschaft SFB 415 (project A3), a Gerok-Fellowship plus intramural funding given to one of the authors, and the MOIN (Molecular Imaging North) research project in Kiel (MOIN-SH) and Hamburg (MOIN-HH).

REFERENCES

1. Schniewind B, Bestmann B, Henne-Bruns D, et al. Quality of life after pancreaticoduodenectomy for ductal adenocarcinoma of the pancreatic head. *Br J Surg.* 2006;93:1099–1107.

2. Lim JE, Chien MW, Earle CC. Prognostic factors following curative resection for pancreatic adenocarcinoma: a population-based, linked database analysis of 396 patients. *Ann Surg.* 2003;237:74–85.
3. Egberts JH, Schniewind B, Sipos B, et al. Superiority of extended neoadjuvant chemotherapy with gemcitabine in pancreatic cancer: a comparative analysis in a clinically adapted orthotopic xenotransplantation model in SCID beige mice. *Cancer Biol Ther.* 2007;6:1227–1232.
4. O'Malley ME, Boland GW, Wood BJ, et al. Adenocarcinoma of the head of the pancreas: determination of surgical unresectability with thin-section pancreatic-phase helical CT. *AJR.* 1999;173:1513–1518.
5. Martin DR, Semelka RC. MR imaging of pancreatic masses. *Magn Reson Imaging Clin N Am.* 2000;8:787–812.
6. DelMaschio A, Vanzulli A, Sironi S, et al. Pancreatic cancer versus chronic pancreatitis: diagnosis with CA 19-9 assessment, US, CT, and CT-guided fine-needle biopsy. *Radiology.* 1991;178:95–99.
7. Delbeke D, Rose DM, Chapman WC, et al. Optimal interpretation of FDG PET in the diagnosis, staging and management of pancreatic carcinoma. *J Nucl Med.* 1999;40:1784–1791.
8. Lemke AJ, Niehues SM, Hosten N, et al. Retrospective digital image fusion of multidetector CT and ^{18}F-FDG PET: clinical value in pancreatic lesions—a prospective study with 104 patients. *J Nucl Med.* 2004;45:1279–1286.
9. Sendler A, Avril N, Helmberger H, et al. Preoperative evaluation of pancreatic masses with positron emission tomography using ^{18}F-fluorodeoxyglucose: diagnostic limitations. *World J Surg.* 2000;24:1121–1129.
10. Pakzad F, Groves AM, Ell PJ. The role of positron emission tomography in the management of pancreatic cancer. *Semin Nucl Med.* 2006;36:248–256.
11. Shields AF, Grierson JR, Dohmen BM, et al. Imaging proliferation in vivo with [F-18]FLT and positron emission tomography. *Nat Med.* 1998;4:1334–1336.
12. Arner ES, Eriksson S. Mammalian deoxyribonucleoside kinases. *Pharmacol Ther.* 1995;67:155–186.
13. Barthel H, Cleij MC, Collingridge DR, et al. 3′-deoxy-3′-[^{18}F]fluorothymidine as a new marker for monitoring tumor response to antiproliferative therapy in vivo with positron emission tomography. *Cancer Res.* 2003;63:3791–3798.
14. Vesselle H, Grierson J, Muzi M, et al. In vivo validation of 3′deoxy-3′-[^{18}F]fluorothymidine ([^{18}F]FLT) as a proliferation imaging tracer in humans: correlation of [^{18}F]FLT uptake by positron emission tomography with Ki-67 immunohistochemistry and flow cytometry in human lung tumors. *Clin Cancer Res.* 2002;8:3315–3323.
15. van Waarde A, Cobben DC, Suurmeijer AJ, et al. Selectivity of ^{18}F-FLT and ^{18}F-FDG for differentiating tumor from inflammation in a rodent model. *J Nucl Med.* 2004;45:695–700.
16. Hara T, Kosaka N, Shinoura N, Kondo T. PET imaging of brain tumor with [methyl-^{11}C]choline. *J Nucl Med.* 1997;38:842–847.
17. Kotzerke J, Prang J, Neumaier B, et al. Experience with carbon-11 choline positron emission tomography in prostate carcinoma. *Eur J Nucl Med.* 2000;27:1415–1419.
18. Kobori O, Kirihara Y, Kosaka N, Hara T. Positron emission tomography of esophageal carcinoma using ^{11}C-choline and ^{18}F-fluorodeoxyglucose: a novel method of preoperative lymph node staging. *Cancer.* 1999;86:1638–1648.
19. Roivainen A, Forsback S, Gronroos T, et al. Blood metabolism of [methyl-^{11}C]choline; implications for in vivo imaging with positron emission tomography. *Eur J Nucl Med.* 2000;27:25–32.
20. Hamacher K, Coenen HH, Stocklin G. Efficient stereospecific synthesis of no-carrier-added 2-[^{18}F]-fluoro-2-deoxy-D-glucose using aminopolyether supported nucleophilic substitution. *J Nucl Med.* 1986;27:235–238.
21. Hara T, Kosaka N, Kishi H. Development of ^{18}F-fluoroethylcholine for cancer imaging with PET: synthesis, biochemistry, and prostate cancer imaging. *J Nucl Med.* 2002;43:187–199.
22. Sipos B, Moser S, Kalthoff H, et al. A comprehensive characterization of pancreatic ductal carcinoma cell lines: towards the establishment of an in vitro research platform. *Virchows Arch.* 2003;442:444–452.
23. Huisman MC, Reder S, Weber AW, Ziegler SI, Schwaiger M. Performance evaluation of the Philips MOSAIC small animal PET scanner. *Eur J Nucl Med Mol Imaging.* 2007;34:532–540.
24. Grutzmann R, Pilarsky C, Ammerpohl O, et al. Gene expression profiling of microdissected pancreatic ductal carcinomas using high-density DNA microarrays. *Neoplasia.* 2004;6:611–622.
25. Sutterluety H, Bartl S, Doetzlhofer A, et al. Growth-regulated antisense transcription of the mouse thymidine kinase gene. *Nucleic Acids Res.* 1998;26:4989–4995.
26. Tommasi S, Pfeifer GP. Constitutive protection of E2F recognition sequences in the human thymidine kinase promoter during cell cycle progression. *J Biol Chem.* 1997;272:30483–30490.
27. Mikulits W, Hengstschlager M, Sauer T, Wintersberger E, Mullner EW. Overexpression of thymidine kinase mRNA eliminates cell cycle regulation of thymidine kinase enzyme activity. *J Biol Chem.* 1996;271:853–860.
28. Kubota R, Yamada S, Kubota K, et al. Intratumoral distribution of fluorine-18-fluorodeoxyglucose in vivo: high accumulation in macrophages and granulation tissues studied by microautoradiography. *J Nucl Med.* 1992;33:1972–1980.
29. Cobben DC, van der Laan BF, Maas B, et al. ^{18}F-FLT PET for visualization of laryngeal cancer: comparison with ^{18}F-FDG PET. *J Nucl Med.* 2004;45:226–231.
30. Yap CS, Czernin J, Fishbein MC, et al. Evaluation of thoracic tumors with ^{18}F-fluorothymidine and ^{18}F-fluorodeoxyglucose-positron emission tomography. *Chest.* 2006;129:393–401.
31. Quon A, Chang ST, Chin F, et al. Initial evaluation of ^{18}F-fluorothymidine (FLT) PET/CT scanning for primary pancreatic cancer. *Eur J Nucl Med Mol Imaging.* October 25, 2007 [E-pub ahead of print].
32. Krieger-Hinck N, Gustke H, Valentiner U, et al. Visualisation of neuroblastoma growth in a Scid mouse model using [^{18}F]FDG and [^{18}F]FLT-PET. *Anticancer Res.* 2006;26:3467–3472.
33. Molthoff CF, Klabbers BM, Berkhof J, et al. Monitoring response to radiotherapy in human squamous cell cancer bearing nude mice: comparison of 2′-deoxy-2′-[^{18}F]fluoro-D-glucose (FDG) and 3′-[^{18}F]fluoro-3′-deoxythymidine (FLT). *Mol Imaging Biol.* 2007;9:340–347.
34. Fueger BJ, Czernin J, Hildebrandt I, et al. Impact of animal handling on the results of ^{18}F-FDG PET studies in mice. *J Nucl Med.* 2006;47:999–1006.
35. Shinoura N, Nishijima M, Hara T, et al. Brain tumors: detection with C-11 choline PET. *Radiology.* 1997;202:497–503.
36. Talbot JN, Gutman F, Fartoux L, et al. PET/CT in patients with hepatocellular carcinoma using [^{18}F]fluorocholine: preliminary comparison with [^{18}F]FDG PET/CT. *Eur J Nucl Med Mol Imaging.* 2006;33:1285–1289.
37. Husarik DB, Miralbell R, Dubs M, et al. Evaluation of [^{18}F]-choline PET/CT for staging and restaging of prostate cancer. *Eur J Nucl Med Mol Imaging.* 2008;35:253–263.
38. Torizuka T, Kanno T, Futatsubashi M, et al. Imaging of gynecologic tumors: comparison of ^{11}C-choline PET with ^{18}F-FDG PET. *J Nucl Med.* 2003;44:1051–1056.
39. Michel V, Yuan Z, Ramsubir S, Bakovic M. Choline transport for phospholipid synthesis. *Exp Biol Med (Maywood).* 2006;231:490–504.
40. Kent C. Regulation of phosphatidylcholine biosynthesis. *Prog Lipid Res.* 1990;29:87–105.